

Electromagnon in the Z-type hexaferrite $(\text{Ba}_x\text{Sr}_{1-x})_3\text{Co}_2\text{Fe}_{24}\text{O}_{41}$

Filip Kadlec,¹ Christelle Kadlec,¹ Jakub Vít,^{1,2} Fedir Borodavka,¹ Martin Kempa,¹
Jan Prokleška,³ Josef Buršík,⁴ Róbert Uhrecký,⁴ Stéphane Rols,⁵ Yi Sheng Chai,⁶
Kun Zhai,⁶ Young Sun,⁶ Jan Drahokoupil,¹ Veronica Goian,¹ and Stanislav Kamba^{1,*}

¹*Institute of Physics, Czech Academy of Sciences,
Na Slovance 2, 182 21 Prague 8, Czech Republic*

²*Faculty of Nuclear Science and Physical Engineering,*

Czech Technical University, Břehová 7, 115 19 Prague 1, Czech Republic

³*Department of Condensed Matter Physics, Faculty of Mathematics and Physics,
Charles University, Ke Karlovu 5, 121 16 Prague 2, Czech Republic*

⁴*Institute of Inorganic Chemistry, Czech Academy of Sciences, 250 68 Řež, Czech Republic*

⁵*Institut Laue-Langevin, Boîte Postale 156, 38042 Grenoble Cedex 9, France*

⁶*Institute of Physics, Chinese Academy of Sciences, Beijing, P. R. China*

(Dated: July 21, 2016)

We studied experimentally the high-temperature magnetoelectric $(\text{Ba}_x\text{Sr}_{1-x})_3\text{Co}_2\text{Fe}_{24}\text{O}_{41}$ prepared as ceramics ($x = 0, 0.2$) and a single crystal ($x = 0.5$) using inelastic neutron scattering, THz time-domain, Raman and far-infrared spectroscopies. The spectra, measured with varying temperature and magnetic field, reveal rich information about the collective spin and lattice excitations. In the ceramics, we observed an infrared-active magnon which is absent in $\mathbf{E}^\omega \perp z$ polarized THz spectra of the crystal, and we assume that it is an electromagnon active in $\mathbf{E}^\omega \parallel z$ polarized spectra. On heating from 7 to 250 K, the frequency of this electromagnon drops from 36 to 25 cm^{-1} and its damping gradually increases, so it becomes overdamped at room temperature. Applying external magnetic field has a similar effect on the damping and frequency of the electromagnon, and the mode is no more observable in the THz spectra above 2 T, as the transverse-conical magnetic structure transforms into a collinear one. Raman spectra reveal another spin excitation with a slightly different frequency and much higher damping. Upon applying magnetic field higher than 3 T, in the low-frequency part of the THz spectra, a narrow excitation appears whose frequency linearly increases with magnetic field. We interpret this feature as the ferromagnetic resonance.

I. INTRODUCTION

The current research on multiferroic materials is motivated by both an incomplete understanding of their fundamental physical properties and their potential in realizing novel devices which would make use of static or dynamic magnetoelectric (ME) coupling in non-volatile memories, spintronics, magnonics and microwave devices. For practical applications, a strong ME coupling near room temperature is required. BiFeO_3 , the most intensively studied multiferroic, exhibits a large ferroelectric (FE) polarization and multiferroicity up to 643 K. However, its spiral magnetic structure persists up to an external magnetic field of 19 T and, therefore, the ME coupling is rather low up to 18 T.¹ Much larger ME coupling was observed in spin-order-induced ferroelectrics.² Unfortunately, most of these materials exhibit multiferroic properties only below ca. 50–100 K. Nevertheless, some ferrites with hexagonal symmetry, called hexaferrites, exhibit magnetic-field-induced electric polarization close to or even far above room temperature and their ME coupling can be very high.^{3–5}

Based on their chemical formulas and crystal structures, hexaferrites can be classified into several types: *M*-type, such as $(\text{Ba}, \text{Sr})\text{Co}_x\text{Ti}_x\text{Fe}_{12-2x}\text{O}_{19}$, *Y*-type $(\text{Ba}, \text{Sr})_2\text{Me}_2\text{Fe}_{12}\text{O}_{22}$, *W*-type $(\text{Ba}, \text{Sr})\text{Me}_2\text{Fe}_{16}\text{O}_{27}$, *Z*-type $(\text{Ba}, \text{Sr})_3\text{Me}_2\text{Fe}_{24}\text{O}_{41}$, *X*-type $(\text{Ba}, \text{Sr})_2\text{Me}_2\text{Fe}_{28}\text{O}_{46}$, and *U*-type $(\text{Ba}, \text{Sr})_4\text{Me}_2\text{Fe}_{36}\text{O}_{60}$, where Me is a biva-

lent metal ion (e.g. Co, Mg, Zn).^{5,6} The structures of hexaferrites can be described as sequences of three basic building blocks (usually denoted by *S*, *R*, and *T*) periodically stacked along the *z* axes. Since the hexagonal structures of hexaferrites are associated with centrosymmetric $P6_3/mmc$ or $R\bar{3}m$ space groups, no FE polarization should exist in these materials. Nevertheless, their ferromagnetic structures are spiral or heliconical and they can be easily changed by external magnetic field to transverse conical, where an electric polarization of the order of tens of $\mu\text{C}/\text{m}^2$ can appear due to the inverse Dzyaloshinskii-Moriya interaction ($\propto \mathbf{S}_i \times \mathbf{S}_j$) between non-parallel spins \mathbf{S}_i and \mathbf{S}_j . In this case the centrosymmetric structure should be broken and the crystal symmetry lowered. Importantly, the magnetic field needed to induce a polarization can be very low (of the order of millitesla) and the effect can be remanent.^{4,7} By contrast, the polarization disappears in higher magnetic fields (usually above 2 T) when the magnetic structure changes.⁵

ME properties of the Z-type hexaferrite $\text{Sr}_3\text{Co}_2\text{Fe}_{24}\text{O}_{41}$ were reported first time by Kitagawa *et al.*⁸ They discovered that this highly resistive material exhibits magnetic-field induced electric polarization at least up to 300 K. ME and magnetodielectric effects in $\text{Sr}_3\text{Co}_2\text{Fe}_{24}\text{O}_{41}$ were confirmed later by other authors.^{9–14} Chun *et al.*³ investigated $(\text{Ba}_x\text{Sr}_{1-x})_3\text{Co}_2\text{Fe}_{24}\text{O}_{41}$ and discovered that the ME effect is the highest in $(\text{Ba}_{0.52}\text{Sr}_{2.48})\text{Co}_2\text{Fe}_{24}\text{O}_{41}$. Moreover, for this composition, the magnetic structure

changes from transverse conical to collinear ferrimagnetic structure at a temperature as high as 400 K, so the ME effect can be measured well above room temperature.^{3,9}

In general, depending on the crystal and magnetic structures, the ME coupling may be due to one of three different mechanisms: exchange striction (magnetostriction $\propto \mathbf{S}_i \cdot \mathbf{S}_j$), inverse Dzyaloshinskii-Moriya interaction or spin-dependent hybridization of the p and d orbitals.² The same mechanisms can be also responsible for the dynamic ME coupling, which activates magnons in the THz or far-infrared *dielectric permittivity* spectra and therefore they are called *electromagnons*.^{2,15,16} By contrast, common magnons impact only upon the magnetic susceptibility spectra in the microwave or THz ranges. They are also called ferromagnetic (FMR) and antiferromagnetic resonances, and their frequencies correspond to acoustic-like and optic-like magnons, respectively, with wavevectors q from the Brillouin-zone center ($q = 0$). As for electromagnons, they have frequently wavevectors out of the Brillouin-zone center ($q \neq 0$) and they can be excited by THz photons (with a wavevector $q \sim 0$) only if the magnetic structure is modulated, which is true in practically all spin-order-induced multiferroics. As regards the hexaferrites, an electromagnon was reported only in the Y-type compound $\text{Ba}_2\text{Mg}_2\text{Fe}_{12}\text{O}_{22}$.¹⁷⁻¹⁹ Interestingly, it was observed not only in the spin-induced FE phase below 50 K, but also in the paraelectric one at 90 K, if an external magnetic field ($0.4 \text{ T} \leq \mu_0 H \leq 1.6 \text{ T}$) was applied; in that case the magnetic structure changed from proper screw to longitudinal (for $\mathbf{H} \parallel z$) or transverse conical (for $\mathbf{H} \perp z$).¹⁸ The activation of the electromagnon in $\mathbf{E}^\omega \parallel z$ polarized spectra was explained by the exchange striction, although the static electric polarization $\mathbf{P} \perp z$ in hexaferrites comes from the inverse Dzyaloshinskii-Moriya interaction.¹⁸

Since the Z-type hexaferrites $(\text{Ba}_x\text{Sr}_{1-x})_3\text{Co}_2\text{Fe}_{24}\text{O}_{41}$ exhibit ferrimagnetic phase transitions at temperatures as high as $T_N = 700 \text{ K}$ and ME coupling up to nearly 400 K, one can expect electromagnons to be activated in their THz spectra at much higher temperatures than in Y-type hexaferrites. For that reason we have performed detailed THz time-domain, infrared (IR), Raman and inelastic neutron scattering (INS) spectroscopic studies from 5 to 900 K on $(\text{Ba}_x\text{Sr}_{1-x})_3\text{Co}_2\text{Fe}_{24}\text{O}_{41}$ ceramics with $x = 0$ and 0.2 and a single crystal with $x = 0.5$. Three spin excitations including one electromagnon were discovered.

II. SAMPLES AND EXPERIMENTAL DETAILS

Powders of hexagonal ferrite with a composition $(\text{Ba}_x\text{Sr}_{1-x})_3\text{Co}_2\text{Fe}_{24}\text{O}_{41}$ ($x = 0$ and 0.2) were prepared by the Pechini type in-situ polymerizable complex method relying on immobilization of metalloorganic precursor complexes in a rigid organic polymer network, thus ensuring the compositional homogeneity of the complex oxide. First, calculated amounts of strontium car-

bonate (SrCO_3), barium carbonate (BaCO_3), cobalt nitrate ($\text{Co}(\text{NO}_3)_2 \cdot 6\text{H}_2\text{O}$), and iron nitrate ($\text{Fe}(\text{NO}_3)_3 \cdot 9\text{H}_2\text{O}$; all chemicals from Sigma-Aldrich) were decomposed in a 0.1 mol/l solution of nitric acid in distilled water. After their complete dissolution, a calculated amount of a polymer gel formed by reaction of citric acid ($\text{HOOCCH}_2\text{C}(\text{OH})-(\text{COOH})\text{CH}_2\text{COOH}$) with ethylene glycol ($\text{HOCH}_2\text{CH}_2\text{OH}$) in water was added to this solution, mixed and heated to 130°C . With continued heating over several hours the clear solution became highly viscous, gradually gelled and finally polymerized into a voluminous resin. After breaking the resin, its drying (at 150°C) and charring (at 350°C) for 24 hrs, the resulting powder was heat-treated in an oxygen atmosphere at 1200°C for 12 hrs. A powder X-ray diffraction measurement proved a single-phase composition of the product. Cold isostatic pressing (pressure 300 MPa) and subsequent sintering at 1200°C in oxygen atmosphere were used to obtain dense ceramics of the Z-phase ferrite. Single- and double-side polished pellets with diameters of 6 mm and thicknesses of 2 and 0.48 mm were prepared for the IR and THz studies, respectively.

A $(\text{Ba}_{0.5}\text{Sr}_{0.5})_3\text{Co}_2\text{Fe}_{24}\text{O}_{41}$ single crystal with a natural hexagonal plane was grown by the flux method.²⁰ It had a diameter of 4–5 mm and a thickness of 1.8 mm.

Low-temperature IR reflectivity measurements in the frequency range $30\text{--}670 \text{ cm}^{-1}$ (or, equivalently, $1\text{--}20 \text{ THz}$) were performed using a Bruker IFS-113v Fourier-transform IR spectrometer equipped with a liquid-He-cooled Si bolometer (1.6 K) serving as a detector. Room-temperature mid-IR spectra up to 5000 cm^{-1} were obtained using a pyroelectric deuterated triglycine sulfate detector.

THz complex transmittance from 3 to 50 cm^{-1} (with the upper limit due to sample opacity) was measured using a custom-made time-domain spectrometer. For the low-temperature IR reflectivity and THz complex transmittance spectroscopy, Oxford Instruments Optistat cryostats with mylar and polyethylene windows, respectively, were used. THz spectroscopy with magnetic field was performed using a custom-made time-domain spectrometer comprising an Oxford Instruments Spectromag cryostat with a superconducting magnet, allowing us to apply an external magnetic field of up to 7 T; the Faraday geometry (wavevector parallel to the magnetic field) was used.

INS was measured on a powder sample (9.75 g) using the neutron time-of-flight spectrometer IN4 in the Institut Laue-Langevin in Grenoble, France.

For Raman studies, a Renishaw RM1000 Micro-Raman spectrometer equipped with a CCD detector and Bragg filters was used. The experiments were performed in the backscattering geometry within the $10\text{--}800 \text{ cm}^{-1}$ range using an Ar laser with the wavelength of 514 nm and an Oxford Instruments Optistat optical continuous He-flow cryostat. Further, using a Quantum design PPMS 9T instrument, we carried out measurements of the magnetic susceptibility, magnetization, and of the

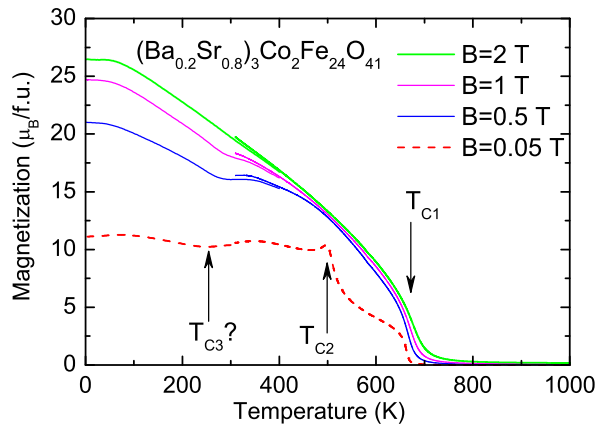


FIG. 1: Temperature dependence of the magnetization for polycrystalline $(\text{Ba}_{0.2}\text{Sr}_{0.8})_3\text{Co}_2\text{Fe}_{24}\text{O}_{41}$ taken at various magnetic fields. The temperatures of magnetic phase transitions are marked by arrows.

ME effect, in a temperature interval from 5 to 1000 K with a magnetic field of up to 9 T.

III. RESULTS AND DISCUSSION

A. Magnetic and magnetoelectric properties

Fig. 1 shows the magnetization M of the $(\text{Ba}_{0.2}\text{Sr}_{0.8})_3\text{Co}_2\text{Fe}_{24}\text{O}_{41}$ ceramics as a function of temperature for several values of magnetic field. These dependences are similar to the previously published data obtained with $\text{Sr}_3\text{Co}_2\text{Fe}_{24}\text{O}_{41}$ ceramics⁸ and a $\text{Ba}_{0.52}\text{Sr}_{2.48}\text{Co}_2\text{Fe}_{24}\text{O}_{41}$ single crystal.³ Thus, the magnetic phase diagram of $(\text{Ba}_x\text{Sr}_{1-x})_3\text{Co}_2\text{Fe}_{24}\text{O}_{41}$ is probably relatively independent of x at least for $0 \leq x \leq 0.2$. The collinear ferrimagnetic structure with spins parallel to the z axis appears below $T_{C1} \approx 700$ K. At $T_{C2} \approx 500$ K, the spins start to rotate towards the xy -plane and at $T_{\text{con}} \approx 400$ K a transverse conical structure is stabilized.³ Near 260–300 K, we observed shallow minima in the $M(T)$ curves, similarly to Refs. 3,9. This feature has not been satisfactorily explained yet, and we suppose it is due to some further changes in the magnetic structure. Subsequently, we measured magnetization curves $M(H)$ at various temperatures (see Fig. 1 in Suppl. Materials²¹) and found some features due to magnetic phase transitions in the range from 0.1 to 1 T. The magnetization reversal processes during these transitions are explained in Ref. 22. ME measurements of $P(H)$ at 10 K (see Fig. 2 in Suppl. Materials²¹) revealed changes in electric polarization induced by magnetic field greater than 0.01 T, attaining a maximum at 0.3 T and vanishing near 2 T. A similar behavior was reported for a single crystal³, where the maximum polarization was, two orders of magnitude higher than in our ceramics. For temperatures higher

than 50 K, a strong leakage conductivity prevented us from acquiring meaningful ME data.

B. Phonon spectra

We performed the factor-group analysis of lattice vibrations in $(\text{Ba},\text{Sr})_3\text{Co}_2\text{Fe}_{24}\text{O}_{41}$ for the centrosymmetric hexagonal space group $P6_3/mmc$ (D_{6h}^4), taking into account the site symmetries published in Refs. 23,24 with the same crystallographic sites shared between Fe/Co and Ba/Sr atoms. The unit cell contains 2×70 atoms, and the analysis yields:

$$\begin{aligned} \Gamma_{D_{6h}^4} = & 29A_{2u}(z) + 37E_{1u}(x, y) + 26A_{1g}(x^2 + y^2, z^2) + \\ & + 33E_{1g}(xz, yz) + 36E_{2g}(x^2 - y^2, xy) + 27B_{2u} + \\ & + 34E_{2u} + 28B_{1g} + 7A_{1u} + 8A_{2g} + 8B_{1u} + 7B_{2g} \end{aligned} \quad (1)$$

where x , y , and z mark electric polarizations of the IR radiation for which the phonons are IR active, whereas the rest of the symbols in parentheses are components of the Raman tensor. After subtracting two acoustic phonons, 64 IR-active and 95 Raman-active phonons are predicted in the spectra. Additional 119 phonons are silent, i.e. inactive in the IR or Raman spectra.

Assuming that the crystal structure undergoes an equitranslational spin-induced FE phase transition, the soft mode in the paraelectric phase should have, according to the tables in Ref. 25, the A_{2u} symmetry, and the resulting acentric space group will be $P6mm$ (C_{6v}^1). The factor-group analysis of phonons from the Brillouin-zone center reads

$$\begin{aligned} \Gamma_{C_{6v}^1} = & 55A_1(z, x^2 + y^2, z^2) + 70E_1(x, y, xz, yz) + 55B_2 \\ & + 70E_2(x^2 - y^2, xy) + 15A_2 + 15B_1. \end{aligned} \quad (2)$$

Thus, in the FE phase, one can expect 123 IR-active modes, 193 modes can be theoretically observed in Raman spectra and 85 modes remain silent. Nevertheless, the intensities of the newly activated modes are expected to be very low, because the polar distortion (proportional to the polarization) in spin-order-induced ferroelectrics and probably also in $(\text{Ba}_x\text{Sr}_{1-x})_3\text{Co}_2\text{Fe}_{24}\text{O}_{41}$ is four orders of magnitude smaller than in the canonical FE BaTiO_3 . We note that, due to this fact, no new phonons below T_C were reported also in other spin-induced ferroelectrics, only small shifts of phonon frequencies were observed due to the spin-phonon coupling.^{26,27} Anyway, the factor-group analysis is useful for the discussion of electromagnon activity in both IR and Raman spectra below.

Fig.2 shows the IR reflectivity spectra of the $(\text{Ba}_{0.2}\text{Sr}_{0.8})_3\text{Co}_2\text{Fe}_{24}\text{O}_{41}$ ceramics and of the $(\text{Ba}_{0.5}\text{Sr}_{0.5})_3\text{Co}_2\text{Fe}_{24}\text{O}_{41}$ single crystal at selected temperatures. The single crystal was grown and polished with the surface normal $[0001]$, therefore only E_{1u} modes are active in its $\mathbf{E}^\omega \parallel x, y$ polarized spectra (\mathbf{E}^ω

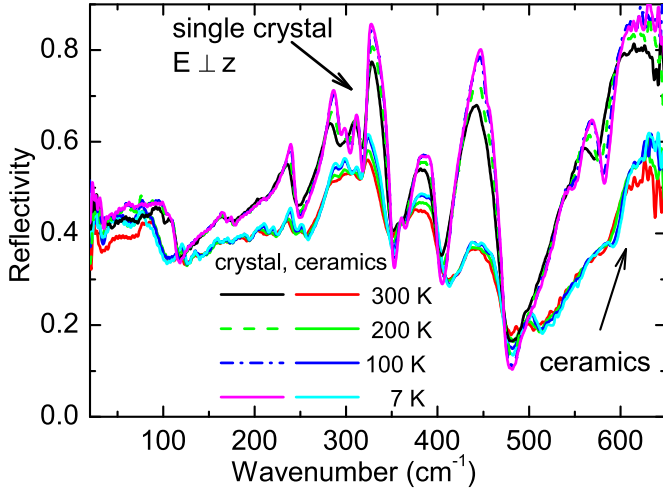


FIG. 2: Temperature dependence of IR reflectivity spectra of $(\text{Ba}_{0.2}\text{Sr}_{0.8})_3\text{Co}_2\text{Fe}_{24}\text{O}_{41}$ ceramics and a $(\text{Ba}_{0.5}\text{Sr}_{0.5})_3\text{Co}_2\text{Fe}_{24}\text{O}_{41}$ single crystal. The latter spectrum was taken in polarization $\mathbf{E}^\omega \perp z$ and $\mathbf{H}^\omega \perp z$, i.e. only E_{1u} symmetry phonons are seen.

denotes the electric vector of the incident radiation). In the spectra of ceramics, both A_{2u} and E_{1u} modes are IR active, but their intensities are reduced. We identified only 21 E_{1u} phonons in the single crystal and 22 phonons in the ceramics, which is much less than expected from the factor-group analysis. The discrepancy is apparently caused by small intensities and/or overlapping of some modes. It is worth noting that no new modes appear in the IR spectra on cooling, i.e. no signature of any structural phase transition is seen below 300 K. The intensities of the reflection bands only increase on cooling due to reduced phonon damping with lowering temperature. The phonon parameters obtained from fits of spectra taken at 10 K are listed in Tab. I in Suppl. Materials.²¹

C. THz studies

Fig. 3 shows complex refractive index spectra of the $(\text{Ba}_{0.2}\text{Sr}_{0.8})_3\text{Co}_2\text{Fe}_{24}\text{O}_{41}$ ceramics obtained by time-domain THz spectroscopy between 7 and 800 K. The low-frequency increase in $n(\omega)$ and $\kappa(\omega)$ occurring above 300 K is due to the sample conductivity arising in the microwave region; furthermore, two clear resonances are seen in the spectra. The higher-frequency one (near $\sim 45 \text{ cm}^{-1}$) is present at all temperatures and it exhibits only a small softening on heating. The lower-frequency one appears at 250 K near 25 cm^{-1} and markedly hardens and sharpens on cooling (its frequency reaches 35 cm^{-1} at 7 K).

Upon applying magnetic field, the lower-frequency resonance broadens, shifts towards lower frequencies and finally disappears at magnetic field values above 2 T. This

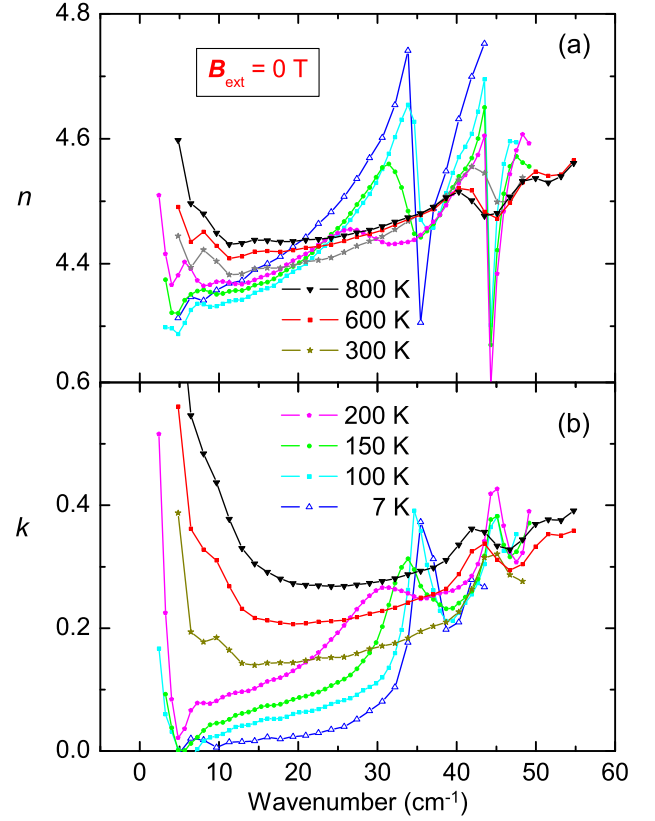


FIG. 3: Spectra of the complex refractive index of the $(\text{Ba}_{0.2}\text{Sr}_{0.8})_3\text{Co}_2\text{Fe}_{24}\text{O}_{41}$ ceramics determined by THz spectroscopy at various temperatures.

behavior is shown in Fig. 4 for 50 K; qualitatively similar magnetic-field dependences were observed at temperatures up to 250 K (see Fig. 3 in Supplement²¹). This is a signature of a magnetic excitation; we assume that it disappears from the spectra due to the magnetic phase transition from the transverse conical to a collinear structure. We expect this mode to remain active up to $T_{\text{con}} \cong 400 \text{ K}$ when the magnetic structure changes. Nevertheless, its damping dramatically increases with temperature, so the mode gradually becomes overdamped. Consequently, above $\sim 250 \text{ K}$, it is seen only as a broad featureless background in the $\kappa(\omega)$ spectra, which overlaps with the conductivity appearing above 300 K (see Fig. 3 in Supplement²¹). Note that the magnetic mode disappears from the THz spectra near the temperature T_{C3} marked in Fig. 1. The mode seen near 45 cm^{-1} is apparently a phonon, because its shape does not change with magnetic field and it remains in the spectra up to the paramagnetic phase.

As the magnetic field is further increased, another narrow excitation appears in the low-frequency part of the THz spectra. Its resonance frequency linearly increases with the magnetic field as $\omega_{\text{FMR}} = \gamma H$ with the proportionality constant $\gamma = 0.032 \text{ THz/T}$ (see inset of Fig. 4), which roughly corresponds to the gyromagnetic ratio of a free electron ($\gamma = 0.028 \text{ THz/T}$). Such behavior is typ-

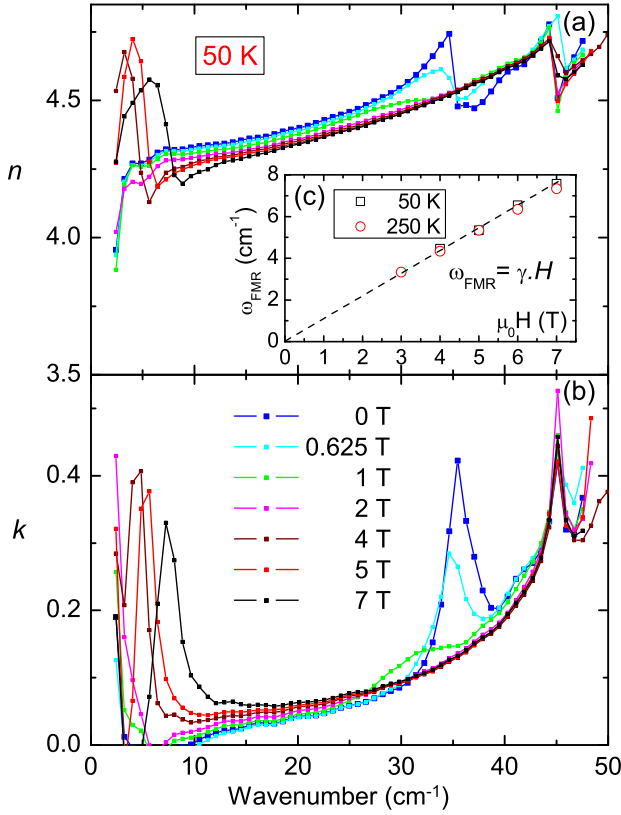


FIG. 4: Magnetic-field dependence of a) index of refraction and b) extinction coefficient in the THz region measured at 50 K. c) Magnetic field dependence of the ferrimagnetic resonance frequency ω_{FMR} in $(\text{Ba}_{0.2}\text{Sr}_{0.8})_3\text{Co}_2\text{Fe}_{24}\text{O}_{41}$ ceramics at 50 and 250 K.

ical of FMRs.²⁸ The same resonance is seen up to 250 K (the highest value attainable in the magnetic cryostat) and at 7 T, for all temperatures, it reaches a frequency of $\approx 7.5 \text{ cm}^{-1}$. (see Fig. 4c and Fig. 3 in Supplement²¹). Without magnetic field, the FMR can be observed in the microwave range. These observations are beyond the scope of the present article and will be presented separately.

In multiferroics, simultaneously magnetically and electrically active spin excitation are called electromagnons. These can be distinguished from magnons by comparing the polarized IR spectra of crystals taken in all possible polarizations. Z-hexaferrite single crystals can be easily grown only in the hexagonal plane, therefore we disposed merely of a (0001) single crystal plate. In Fig. 5, polarized THz spectra of the $(\text{Ba}_{0.5}\text{Sr}_{0.5})_3\text{Co}_2\text{Fe}_{24}\text{O}_{41}$ single crystal with $\mathbf{E}^\omega \perp z \perp \mathbf{H}^\omega$ (\mathbf{H}^ω denoting the magnetic vector of the incident beam) are compared with the spectra of ceramics. In the single crystal, we observed a very weak and narrow excitation at 31 cm^{-1} . Since this mode is independent of temperature and external magnetic field (not shown) and its frequency is clearly lower than that of the magnetic excitation in ceramics, we interpret it as a weak phonon with the E_{1u} symme-

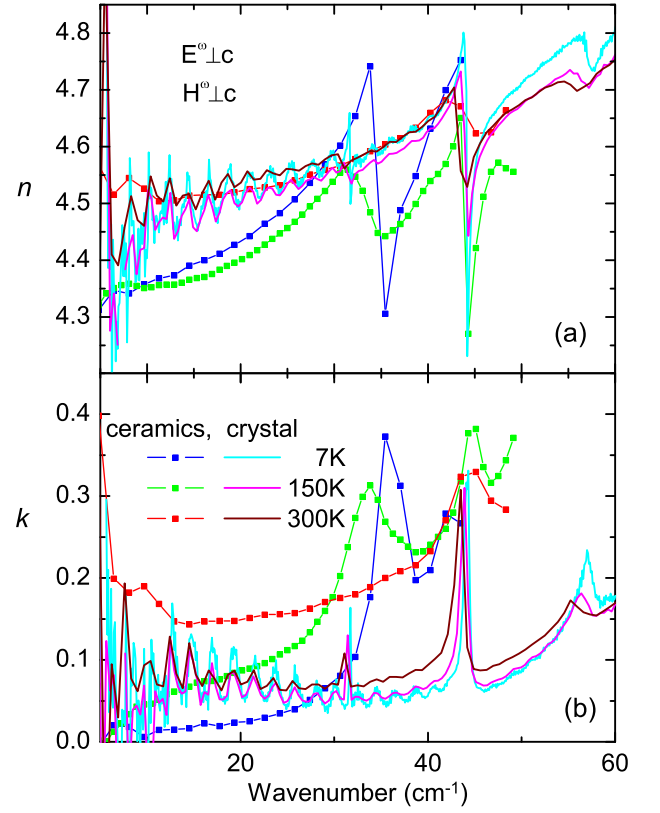


FIG. 5: Comparison of THz spectra of a) index of refraction and b) extinction coefficient in $(\text{Ba}_{0.2}\text{Sr}_{0.8})_3\text{Co}_2\text{Fe}_{24}\text{O}_{41}$ ceramics and $(\text{Ba}_{0.5}\text{Sr}_{0.5})_3\text{Co}_2\text{Fe}_{24}\text{O}_{41}$ single crystal at three temperatures. The spectra of the single crystal are polarized $\mathbf{E}^\omega \perp z \perp \mathbf{H}^\omega$, but the [0001] crystal plane was tilted by 6° from the sample surface, therefore the narrow weak mode near 44 cm^{-1} is probably a leakage phonon mode from the $\mathbf{E}^\omega \parallel z$ polarized spectra. The oscillations in the spectra of the single crystal are artifacts due to echoes from multiple reflections in the sample. They can be avoided by time windowing, but then the spectral resolution is lower and the peak near 32 cm^{-1} is not resolved.

try. As the spin excitation near 36 cm^{-1} is not active in the $(\mathbf{E}^\omega \perp z; \mathbf{H}^\omega \parallel z)$ polarized THz spectra²⁹, it must be an electromagnon active for $\mathbf{E}^\omega \parallel z$. The existence of this electromagnon was reported already in 2014 at the March APS meeting by Chun²⁹ but never published.

The two excitations near 44 and 57 cm^{-1} are phonons. The former one is much weaker than the corresponding phonon in ceramics, so it is probably due to a leakage of an $A_{2u}(z)$ mode.

THz spectra of the $(\text{Ba}_{0.5}\text{Sr}_{0.5})_3\text{Co}_2\text{Fe}_{24}\text{O}_{41}$ single crystal measured in external magnetic field (not shown) revealed a FMR below 10 cm^{-1} with a frequency identical with that of the FMR in ceramics (see Fig. 4). This provides an evidence that the FMR has a magnon-like character and that it is active in the $\mathbf{E}^\omega \perp z \perp \mathbf{H}^\omega$ polarized THz spectra.

THz spectra of $\text{Sr}_3\text{Co}_2\text{Fe}_{24}\text{O}_{41}$ ceramics revealed the same excitations like in $(\text{Ba}_{0.2}\text{Sr}_{0.8})_3\text{Co}_2\text{Fe}_{24}\text{O}_{41}$, i.e.,

a phonon near 45 cm^{-1} and an electromagnon near 35 cm^{-1} , (see Fig. 4 in Supplement²¹) which vanishes from the spectra at 250 K. This provides an evidence that the crystalline and magnetic structures of both samples are almost identical. This was also confirmed by very recent magnetic studies of $(\text{Ba}_x\text{Sr}_{1-x})_3\text{Co}_2\text{Fe}_{24}\text{O}_{41}$ with x ranging from 0 to 1.²²

D. Raman scattering

In the non-centrosymmetric FE phases, the electromagnons have to be both IR and Raman active, similarly to the case of BiFeO_3 .³⁰ In our case, the electromagnon is active in the $\mathbf{E}^\omega \parallel z$ -polarized THz spectra, so if the structure is FE (space group $P6mm$), according to the selection rules in Eq. (2), the electromagnon has the A_1 symmetry and it should be also Raman active in the z^2 -polarized spectra.

We measured temperature-dependent Raman spectra of the single crystal (Fig. 6) and ceramics (see Fig. 5 in Supplement²¹) on cooling down to 4 K. Indeed, below 250 K, a distinctive excitation appears in the low-frequency part of the spectra. The inset of Fig. 6 compares the temperature dependences of frequencies of the Raman-active excitations in the single crystal and ceramics with those of the IR active electromagnon in ceramics. The frequencies of all three excitations are very similar and all of them decrease on heating towards T_{con} . Nevertheless, a detailed analysis reveals some differences: (i) The Raman-active mode seen in the ceramics has a frequency systematically higher by $7\text{--}10\text{ cm}^{-1}$ than the IR-active one observed in the same sample. (ii) Upon heating, the Raman-active mode detected in the single crystal softens faster than those in ceramics. (iii) In both samples, the Raman-active spin excitation has a damping systematically 2–3 times higher than the IR-active mode.

The first difference can be possibly a consequence of an angular dependence of the mode frequency (oblique mode) relevant to the single-crystalline ceramic grains (in fact, this Raman mode was observed only in few grains, and we suppose that their z crystal axes were oriented almost parallel to the sample surface). The second observation could be theoretically owing to somewhat different Ba concentrations in the ceramics ($x = 0.2$) and the single crystal ($x = 0.5$), but since we know that the magnetic structure is identical for both compositions, this possibility is not likely. Instead, we note that owing to the sintering, there may be a varying mechanical stress, which may influence the temperature dependences of the mode frequencies in the individual grains. Finally, the different dampings of the modes in Raman and THz spectra do not support the idea of identical modes either. Consequently, we are not sure that the spin excitations seen in both THz and Raman spectra are the same. In case the Raman mode is not identical with the IR-active one, the Raman mode could be due to an antiferromag-

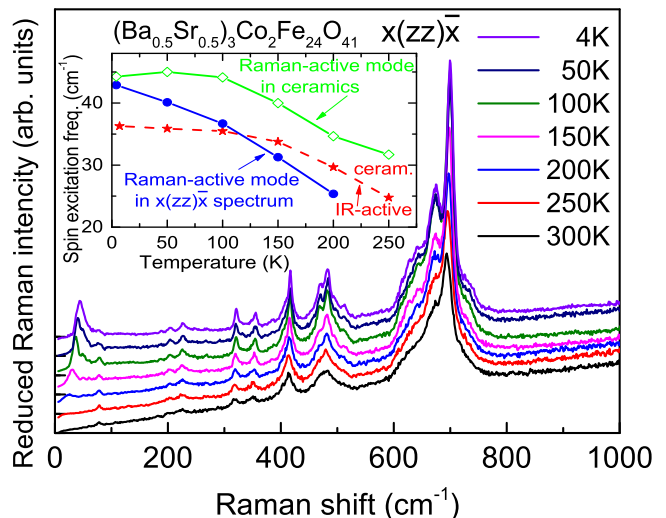


FIG. 6: Temperature dependence of $x(zz)\bar{x}$ Raman spectra of the $(\text{Ba}_{0.5}\text{Sr}_{0.5})_3\text{Co}_2\text{Fe}_{24}\text{O}_{41}$ single crystal. The inset shows the temperature dependence of spin excitation frequencies obtained from these spectra and from unpolarized Raman and THz spectra of the $(\text{Ba}_{0.2}\text{Sr}_{0.8})_3\text{Co}_2\text{Fe}_{24}\text{O}_{41}$ ceramics.

netic resonance or more probably multi-magnon scattering involving magnons with the highest magnon density of states (DOS).

In the opposite case, if the Raman and IR-active excitations corresponded to the same vibrational mode, it would be an argument supporting the FE $P6mm$ crystal symmetry of the Z-hexaferrite. Then, the FE polarization \mathbf{P} would be oriented along the z axis, which is in contradiction with Ref. 3, where magnetic-field induced changes in polarization in the hexagonal plane were observed. One might also hypothetically assume that at zero magnetic field, $\mathbf{P} \parallel z$, and that \mathbf{P} tilts away from the z axis in external magnetic field; in such a case, the crystal structure would change to monoclinic. However, in the FE phase, a much higher number of phonons than observed should be present in both IR and Raman spectra. For example, at 4 K, we resolved 20 modes in z^2 -polarized Raman spectra and 21 IR-active phonons in $\mathbf{E}^\omega \perp z$ spectra. These numbers are in better agreement with the 26 $A_{1g}(z^2)$ and 36 $E_{1u}(x, y)$ modes predicted for the paraelectric $P6_3/mmc$ phase than with the 54 $A_1(z^2)$ and 70 $E_1(x, y)$ modes expected for the FE $P6mm$ symmetry.

We can conclude that our spectra do not support any FE distortion in zero magnetic field. This is in agreement with the known literature; up to now, in the structural studies of Z-hexaferrite $(\text{Ba}_x\text{Sr}_{1-x})_3\text{Co}_2\text{Fe}_{24}\text{O}_{41}$, no polar space group was resolved^{23,24} and the electric polarization $\mathbf{P} \perp z$ was observed only in an external magnetic field.^{3,8} Nevertheless, for final proving or disproving of the polar crystal structure, we propose further complementary experiments, such as second-harmonic generation or high-resolution electron diffraction.

E. Inelastic neutron scattering

Some electromagnons activated in the THz dielectric spectra by exchange coupling have wavevectors from the Brillouin-zone boundary,^{31–33} where the magnon DOS attains a maximum. Such magnons should be recognized by the corresponding maxima of intensity in the INS spectra. Using the powder, we have performed INS experiments with various energy resolutions. Fig. 7a shows a map representing the orientation-averaged scattering intensity at $T = 5$ K. The high INS intensity seen as a column at $Q \approx 4 \text{ \AA}^{-1}$ and for all Q at energies above 15 meV corresponds to the phonon DOS. Near the neutron momentum transfer value of $Q = 1.3 \text{ \AA}^{-1}$, a magnetically active branch (marked by the dashed line) extends in energy up to at least 20 meV. The magnon DOS (proportional to the scattering intensity integrated over the interval $1.2 \leq Q \leq 1.4 \text{ \AA}^{-1}$) exhibits a small maximum near $8 \text{ meV} \approx 64 \text{ cm}^{-1}$ (see Fig. 7b). Near this energy we see only a weak excitation in the $\mathbf{E}^\omega \perp z$ polarized IR reflectivity spectra (see Fig. 2 and Tab. I in Supplement²¹); based solely on our data, we cannot decide whether this is an electromagnon or a phonon. The electromagnon energy, according to our THz spectra, amounts to 4–5.5 meV, but at the low temperatures used in INS experiments, at this energy transfer value, a minimum in magnon DOS is seen (Fig. 7b). Subsequently, the wavevector of the electromagnon is most probably not from the Brillouin zone center or boundary. This is rather surprising because recent polarized INS studies of a Y-type hexaferrite claimed that the observed electromagnon with similar features as the one in Z-hexaferrite was a zone-center mode.¹⁹

In the transverse-conical structure, the electromagnon can induce an oscillating electric polarization along the z axis. Therefore we suggest that it is activated by the exchange-striction mechanism. Note that in both Z- and Y-type hexaferrites, the static polarization \mathbf{P} appears due to the inverse Dzyaloshinskii-Moriya interaction^{2,8} perpendicularly to the z axis, if one applies an external magnetic field $\mathbf{H} \perp z$ whereby the transverse conical structure is stabilized.^{3,19} However, the magnetic structure of the Y-type hexaferrite is longitudinally conical at $\mu_0 H = 0 \text{ T}$,^{17,18} whereas that of the Z-hexaferrite at zero and small magnetic fields is transverse conical. The electromagnons in both materials share several features: (i) they are active in $\mathbf{E}^\omega \parallel z$ even in zero magnetic field, (ii) their frequencies shift with external magnetic field and, finally, (iii) they disappear from the spectra above some threshold magnetic field, when the transverse or longitudinal conical magnetic structures disappear.

IV. CONCLUSION

In conclusion, by using several complementary spectroscopic techniques, we have obtained a comprehensive set of information on the spin and lattice dynamics of the

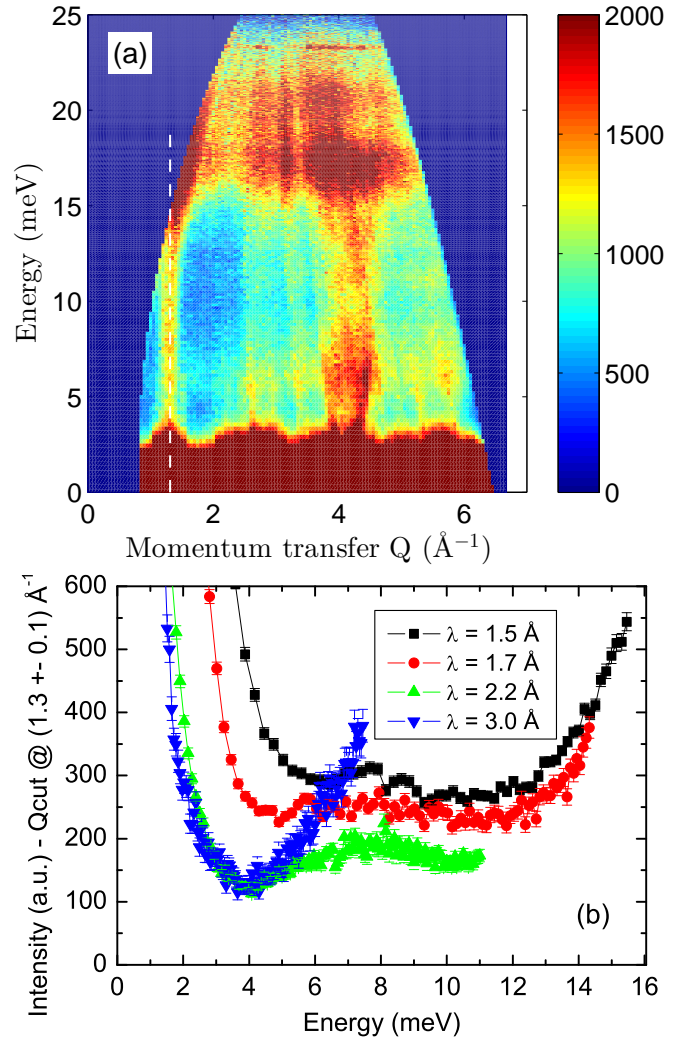


FIG. 7: (a) INS intensity as a function of momentum and energy transfers, measured on $(\text{Ba}_{0.2}\text{Sr}_{0.8})_3\text{Co}_2\text{Fe}_{24}\text{O}_{41}$ at 5 K. The dashed line marks the signal corresponding to the magnon branch. The remaining signal comes from phonon DOS. The energy resolution was $\Delta E = 1.5 \text{ meV}$, the wavelength of the incident neutrons was 1.5 \AA . (b) Magnon DOS calculated from the INS spectra for $1.2 \leq Q \leq 1.4 \text{ \AA}^{-1}$ taken with various wavelengths λ of the incident neutrons.

Z-type hexaferrite compounds $(\text{Ba}_x\text{Sr}_{1-x})_3\text{Co}_2\text{Fe}_{24}\text{O}_{41}$, in broad frequency and temperature ranges.

In the low-temperature THz spectra of $(\text{Ba}_x\text{Sr}_{1-x})_3\text{Co}_2\text{Fe}_{24}\text{O}_{41}$ ceramics, a soft spin excitation near 35 cm^{-1} was discovered, whose frequency softens on heating towards $T_{\text{con}} \approx 400 \text{ K}$ and its damping increases. An external magnetic field exceeding 2 T induces a change of magnetic structure and the spin excitation vanishes from the THz spectra. THz spectra obtained on a single crystal revealed the same magnon in the $\mathbf{E}^\omega \parallel z$ polarized spectra, therefore we claim that it is an electromagnon. Since the excitation is observed in the transverse conical magnetic structure, we propose that it is activated by the exchange striction mechanism.

A spin excitation with a similar frequency was discovered in Raman spectra. Should it be the same electromagnon, the sample would be FE with a polarization $\mathbf{P} \parallel z$ and the $P6mm$ space group. This is rather unlikely, because up to now, only $\mathbf{P} \perp z$ oriented polarization was observed and the numbers of phonon modes observed in the IR and Raman spectra are much lower than those allowed in the FE phase. Nevertheless, further structural, magnetoelectric and second-harmonic-generation experiments appear necessary to clearly prove or disprove a polar phase in $(\text{Ba}_x\text{Sr}_{1-x})_3\text{Co}_2\text{Fe}_{24}\text{O}_{41}$.

Upon applying magnetic field higher than 3 T, in the low-frequency part of the THz spectra, a narrow excitation appears whose frequency linearly increases with magnetic field. Its behavior is independent on temperature (investigated up to 250 K) and since the proportion-

ality constant of the resonance frequency on the magnetic field corresponds to the gyromagnetic ratio of a free electron, we interpret this excitation as the ferromagnetic resonance.

Acknowledgments

This work was supported by the Czech Science Foundation projects 15-08389S and 14-18392S, the program of Czech Research Infrastructures, project LM2011025 and MŠMT project LD15014. The experiments in ILL Grenoble were carried out within the project LG14037 financed by the Ministry of Education of the Czech Republic.

-
- * Authors to whom correspondence should be addressed; e-mail: kamba@fzu.cz; kadlec@fzu.cz
- ¹ M. Tokunaga, M. Azuma, and Y. Shimakawa, J. Phys. Soc. Jpn. **79**, 064713 (2010).
 - ² Y. Tokura, S. Seki, and N. Nagaosa, Rep. Prog. Phys. **77**, 076501 (2014).
 - ³ S. H. Chun, Y. S. Chai, B.-G. Jeon, H. J. Kim, Y. S. Oh, I. Kim, H. Kim, B. J. Jeon, S. Y. Haam, J.-Y. Park, et al., Phys. Rev. Lett. **108**, 177201 (2012).
 - ⁴ Y. S. Chai, S. Kwon, S. H. Chun, I. Kim, B.-G. Jeon, K. H. Kim, and S. Lee, Nature Commun. **5**, 4208 (2014).
 - ⁵ T. Kimura, Annu. Rev. Cond. Matt. Phys. **3**, 93 (2012).
 - ⁶ R. C. Pullar, Prog. Mat. Sci. **57**, 1191 (2012).
 - ⁷ S. Shen, L. Yan, Y. Chai, J. Cong, and Y. Sun, Appl. Phys. Lett. **104**, 032905 (2014).
 - ⁸ Y. Kitagawa, Y. Hiraoka, T. Honda, T. Ishikura, H. Nakamura, and T. Kimura, Nature Mat. **9**, 797 (2010).
 - ⁹ M. Soda, T. Ishikura, H. Nakamura, Y. Wakabayashi, and T. Kimura, Phys. Rev. Lett. **106**, 087201 (2011).
 - ¹⁰ J. Wu, Z. Shi, J. Xu, N. Li, Z. Zheng, H. Geng, Z. Xie, and L. Zheng, Appl. Phys. Lett. **101**, 122903 (2012).
 - ¹¹ X. Zhang, Y. G. Zhao, Y. F. Cui, L. D. Ye, J. W. Wang, S. Zhang, H. Y. Zhang, and M. H. Zhu, Appl. Phys. Lett. **100**, 032901 (2012).
 - ¹² K. Ebnabbasi, M. Mohebbi, and C. Vittoria, Appl. Phys. Lett. **101**, 062406 (2012).
 - ¹³ K. Ebnabbasi, Y. Chen, A. Geiler, V. Harris, and C. Vittoria, J. Appl. Phys. **111**, 07 (2012).
 - ¹⁴ K. Okumura, K. Haruki, T. Ishikura, S. Hirose, and T. Kimura, App. Phys. Lett. **103**, 032906 (2013).
 - ¹⁵ A. Pimenov, A. Mukhin, V. Y. Ivanov, V. Travkin, A. Balbashov, and A. Loidl, Nature Phys. **2**, 97 (2006).
 - ¹⁶ N. Kida, Y. Takahashi, J. Lee, R. Shimano, Y. Yamasaki, Y. Kaneko, S. Miyahara, N. Furukawa, T. Arima, and Y. Tokura, J. Opt. Soc. Am. B **26**, A35 (2009).
 - ¹⁷ N. Kida, D. Okuyama, S. Ishiwata, Y. Taguchi, R. Shimano, K. Iwasa, T. Arima, and Y. Tokura, Phys. Rev. B **80**, 220406(R) (2009).
 - ¹⁸ N. Kida, S. Kumakura, S. Ishiwata, Y. Taguchi, and Y. Tokura, Phys. Rev. B **83**, 064422 (2011).
 - ¹⁹ T. Nakajima, Y. Takahashi, S. Kibayashi, M. Matsuda, K. Kakurai, S. Ishiwata, Y. Taguchi, Y. Tokura, and T. Arima, Phys. Rev. B **93**, 035119 (2016).
 - ²⁰ N. Momozawa, M. Mita, and H. Takei, J. Cryst. Growth **83**, 403 (1987).
 - ²¹ See supplementary material at <https://link.aps.org/supplemental/...> (????).
 - ²² R. Tang, C. Jiang, H. Zhou, and H. Yang, J. Alloys Comp. **658**, 132 (2016).
 - ²³ Y. Takada, T. Tachibana, T. Nakagawa, T. Yamamoto, T. Shimada, and S. Kawano, J. Jpn. Soc. Powder Powder Metallurgy **50**, 618 (2003).
 - ²⁴ Y. Takada, T. Nakagawa, M. Tokunaga, Y. Fukuta, T. Tanaka, T. A. Yamamoto, T. Tachibana, S. Kawano, Y. Ishii, and N. Igawa, J. Appl. Phys. **100**, 043904 (2006).
 - ²⁵ V. Janovec, V. Dvořák, and J. Petzelt, Czech. J. Phys. **25**, 1362 (1975).
 - ²⁶ M. Schmidt, C. Kant, T. Rudolf, F. Mayr, A. A. Mukhin, A. M. Balbashov, J. Deisenhofer, and A. Loidl, Eur. Phys. J. B **71**, 411 (2009).
 - ²⁷ T. Möller, P. Becker, L. Bohatý, J. Hemberger, and M. Grüninger, Phys. Rev. B **90**, 155105 (2014).
 - ²⁸ C. Kittel, *Introduction to Solid State Physics* (John Wiley and Sons, Eighth Edition, 2004).
 - ²⁹ S. H. Chun, lecture at APS March Meeting, Denver, URL: <https://absuploads.aps.org/presentation.cfm?pid=10935> (2014).
 - ³⁰ S. Skiadopoulou, V. Goian, C. Kadlec, F. Kadlec, X. F. Bai, I. C. Infante, B. Dkhil, C. Adamo, D. G. Schlom, and S. Kamba, Phys. Rev. B **91**, 174108 (2015).
 - ³¹ M. P. V. Stenberg and R. de Sousa, Phys. Rev. B **80**, 094419 (2009).
 - ³² M. P. V. Stenberg and R. de Sousa, Phys. Rev. B **85**, 104412 (2012), *ibid.* **80**, 094419 (2009).
 - ³³ C. Kadlec, F. Kadlec, V. Goian, M. Gich, M. Kempa, S. Rols, M. Savinov, J. Prokleška, M. Orlita, and S. Kamba, Phys. Rev. B **88**, 104301 (2013).

**V. ELECTROMAGNON IN Z-TYPE
HEXAFERRITE $(\text{Ba}_x\text{Sr}_{1-x})_3\text{Co}_2\text{Fe}_{24}\text{O}_{41}$ -
SUPPLEMENTARY MATERIALS**

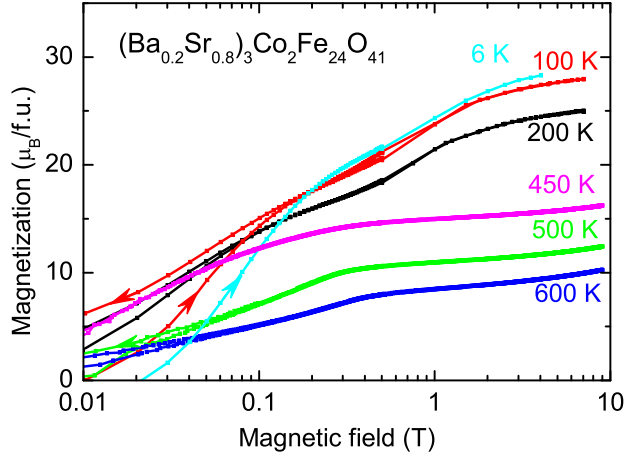


FIG. 1: Magnetization curves of polycrystalline $(\text{Ba}_{0.2}\text{Sr}_{0.8})_3\text{Co}_2\text{Fe}_{24}\text{O}_{41}$ taken at various temperatures.

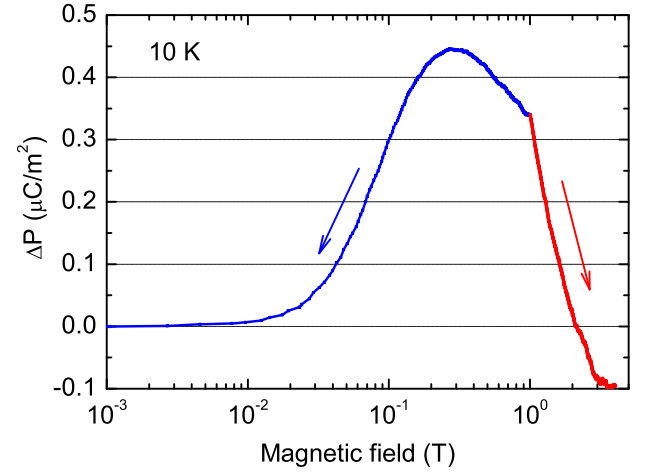


FIG. 2: Magnetic-field dependence of polarization changes at $T = 10$ K for the $(\text{Ba}_{0.2}\text{Sr}_{0.8})_3\text{Co}_2\text{Fe}_{24}\text{O}_{41}$ ceramics. The blue and red curves show changes upon decreasing and increasing magnetic field, respectively.

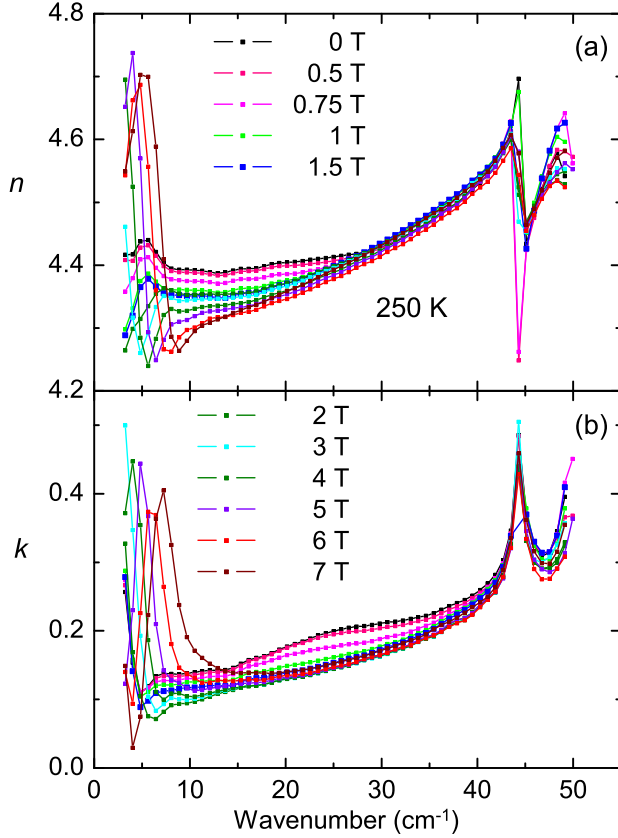


FIG. 3: Magnetic-field dependence of a) index of refraction and b) extinction coefficient of $(\text{Ba}_{0.2}\text{Sr}_{0.8})_3\text{Co}_2\text{Fe}_{24}\text{O}_{41}$ ceramics measured at 250 K.

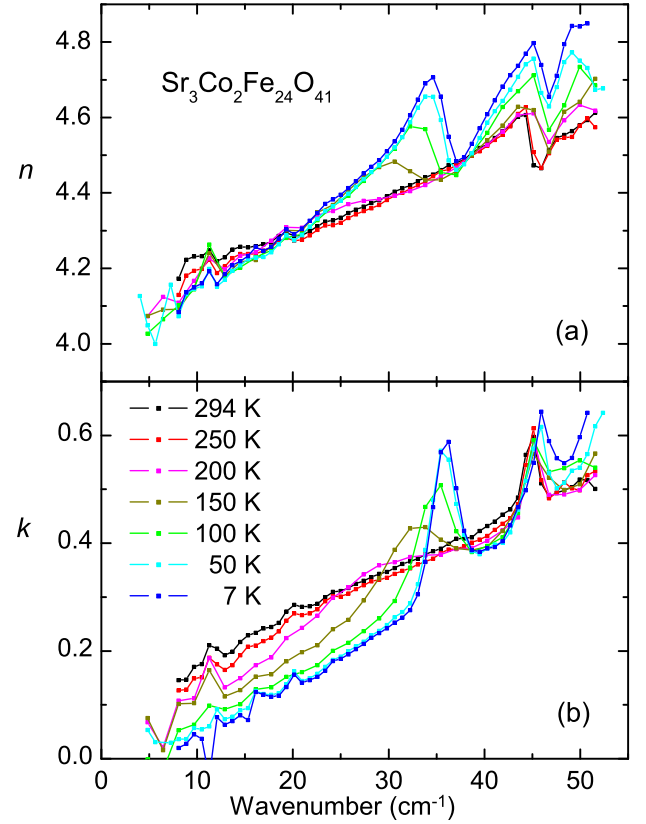


FIG. 4: Temperature dependence of THz spectra of the complex refractive index of $\text{Sr}_3\text{Co}_2\text{Fe}_{24}\text{O}_{41}$ ceramics

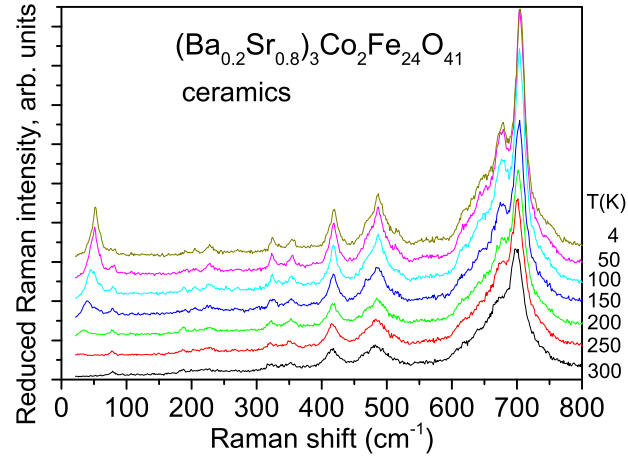


FIG. 5: Temperature dependence of Raman spectra of the $(\text{Ba}_{0.2}\text{Sr}_{0.8})_3\text{Co}_2\text{Fe}_{24}\text{O}_{41}$ ceramics measured with the polarizer and analyzer set parallel. It is important to stress that the electromagnon seen below 50 cm^{-1} was observed only in few ceramic grains. This is consistent with its activity only in the z^2 Raman spectra. The grains are randomly oriented and only few of them have their z axes lying in the sample plane.

TABLE I: Comparison of phonon fitting parameters describing IR reflectivity and THz transmission spectra of $(\text{Ba}_{0.2}\text{Sr}_{0.8})_3\text{Co}_2\text{Fe}_{24}\text{O}_{41}$ ceramics and those of the $(\text{Ba}_{0.5}\text{Sr}_{0.5})_3\text{Co}_2\text{Fe}_{24}\text{O}_{41}$ single crystal ($\mathbf{E}^\omega \perp z$ and $\mathbf{H}^\omega \perp z$) obtained at $T = 10$ K. The high-frequency contributions to permittivity were $\varepsilon_\infty = 4.92$ in the ceramics and $\varepsilon_\infty = 4.79$ in the single crystal. The phonons seen in the IR reflectivity spectra of the single crystal are assumed to have the E_{2u} symmetry. The two phonons in THz transmission spectra below 60 cm^{-1} are much weaker in the crystal than in the ceramics, therefore we assume they have the A_{2u} symmetry and they appear as a leakage from the $\mathbf{E}^\omega \parallel z$ spectra (the z crystal axis was tilted by 6° from the normal crystal plane). The oscillators present only in the ceramics are assumed to have the A_{2u} symmetry.

Symmetry	Ceramics			Single crystal		
	$\omega_{\text{TO}} (\text{cm}^{-1})$	$\gamma_{\text{TO}} (\text{cm}^{-1})$	$\Delta\varepsilon$	$\omega_{\text{TO}} (\text{cm}^{-1})$	$\gamma_{\text{TO}} (\text{cm}^{-1})$	$\Delta\varepsilon$
$A_{2u}?$	45.26	1.69	0.12	43.78	0.24	0.02
$A_{2u}?$				56.91	1.92	0.04
E_{2u}				66.33	9.19	0.24
	87.09	29.80	4.03			
E_{2u}				98.43	19.29	1.80
E_{2u}				109.56	10.83	0.82
A_{2u}	123.04	8.29	0.33			
A_{2u}	138.23	8.65	0.15			
E_{2u}	160.06	15.62	0.18	166.91	8.79	0.24
E_{2u}	172.04	11.37	0.17	176.32	9.32	0.21
A_{2u}	190.02	17.04	0.36			
E_{2u}	211.84	14.00	0.46	209.70	28.11	0.68
A_{2u}	222.54	7.28	0.14			
E_{2u}	240.52	12.85	0.54	239.23	11.88	1.70
A_{2u}	252.93	11.33	0.30			
				267.91	29.74	0.89
E_{2u}	285.88	13.01	0.77	285.02	8.46	2.01
E_{2u}	298.72	16.58	1.31	297.01	11.34	0.89
E_{2u}	309.85	6.11	0.10	309.85	12.21	1.22
E_{2u}	320.97	17.47	1.30	323.54	4.62	1.01
E_{2u}	359.49	6.46	0.05	358.83	11.09	0.22
E_{2u}				374.90	15.91	0.59
E_{2u}	373.18	42.74	1.53	385.81	23.89	0.50
E_{2u}				431.25	9.52	1.04
A_{2u}	503.29	20.03	0.08			
E_{2u}	540.95	12.12	0.02	539.23	27.63	0.79
E_{2u}	566.62	59.22	0.81	560.49	21.00	0.64
E_{2u}	595.73	36.54	0.33	590.59	14.14	0.38